Improving the Binding Characteristics of Tripodal Compounds on Single Layer Graphene

Jason A. Mann and William R. Dichtel*

Department of Chemistry and Chemical Biology, Baker Laboratory, Cornell University, Ithaca, New York 14853-1301, United States

ABSTRACT Graphene is an atomically thin, transparent, and conductive electrode material of interest for sensors and energy conversion and storage devices, among others. Fully realizing its potential will require robust and general methods to anchor active functionality onto its pristine basal plane. Such strategies should not utilize covalent bond formation, which disrupts the graphene's π-electron system, from which most of its desirable properties arise.

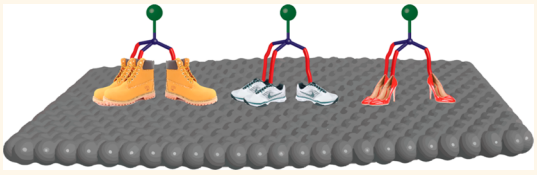

We recently introduced a tripodal binding motif, which forms robust monolayers on graphene capable of immobilizing active proteins and preventing their denaturation. Here we describe structure−property relationships for a series of tripod binding groups with "feet" of different sizes. Each derivative adsorbs strongly ($\Delta G_{ads} \approx -39$ kJ mol^{-1}) to graphene's basal plane, yet the resulting monolayers exhibit kinetic stabilities that vary over 2 orders of magnitude and molecular densities that vary by a factor of 2. This study identifies phenanthrene as a superior anchor relative to pyrene on the basis of its increased monolayer density and similar kinetic stability. We also demonstrate that varying the length of the methylene linkers between the feet and tripodal core does not affect binding substantially. These results represent the first demonstration of structure−property relationships in the assembly of molecular adsorbates on graphene and provide a paradigm for designing effective graphene binding motifs.

KEYWORDS: self-assembly · monolayer · electrochemistry · graphene electrode · functionalization · noncovalent · cobalt bis-terpyridine

Graphene offers a combination of useful properties found in no other single material and has attracted intense research interest since the isolation of single-layer samples by mechanical exfoliation in 2004.[1] Both single-layer (SLG) and few-layer graphene (FLG) exhibit exceptional conductivity,[2] high strength and flexibility,[3] optical transparency,[4−6] and impermeability to atomic and molecular species.[7−9] Recent advances in graphene production, most notably using chemical vapor deposition (CVD) techniques, provide high quality,[10] large-area[11] samples that are readily transferred to arbitrary substrates.[12−17] SLG's increased availability and exceptional properties have inspired the development of general methods to interface molecular[18−27] and polymeric[28−32] species to its basal plane. These strategies are only now emerging as compared to the established self-assembled monolayer chemistries available for metallic (*e.g.*, Au, Ag, and Pt),[33] metal oxide (*e.g.*, indium-doped tin oxide),[34−36] and Si electrodes.[37] Covalent functionalization of graphene has been achieved using diazonium reagents,[38−42] but these reactions occur preferentially at edges and defect sites[43,44] and degrade graphene's desirable properties at high functionalization densities.[45−47] Noncovalent functionalization avoids these undesirable features, which has motivated our efforts to design compounds that form predictable and robust self-assembled monolayers on SLG.

We recently introduced a tripodal graphene binding motif that binds multivalently to the SLG surface through three pyrene "feet".[48] Monolayers of these tripods form on SLG from dilute (μM) solutions and are 10^3 times more kinetically stable than those of comparable monovalent binding groups. The noncovalent interactions between the tripods and SLG permit molecular diffusion over the surface, which was characterized using scanning electrochemical microscopy.[49] Furthermore, tripod monolayers capable of protein bioconjugation serve as effective anchors that preserve the function of attached antibodies[50] and lectin proteins.[51] In contrast, these proteins denature and lose their molecular recognition

* Address correspondence to wdichtel@cornell.edu.

Received for review May 22, 2013 and accepted July 16, 2013.

Published online July 16, 2013
10.1021/nn402599x

functions when adsorbed onto bare SLG or SLG functionalized with a monolayer of monovalent pyrene anchors. The above findings motivated us to improve the tripod binding characteristics by exploring the influence of different binding groups on their molecular packing density and monolayer stability.

Here we show that tripods bearing phenanthrene and naphthalene "feet" form monolayers with higher molecular density than the pyrene tripod, consistent with their smaller binding groups. However, they show reduced resistance to desorption when exposed to organic solvents under infinite dilution conditions. For example, naphthalene tripods form monolayers with 1.54 times higher density than pyrene tripods, but desorb 2.5 orders of magnitude more rapidly. This trade-off suggests that the binding area of naphthalene tripods is too small to be of practical use for many applications, although their packing density and stability are superior to those of single pyrene moieties. In contrast, phenanthrene tripods offer a comparable increase in molecular density (1.43 times that of pyrene tripods) and desorb only three times as quickly. As such, phenanthrene tripods are likely to serve as ideal binding groups for many applications. Comparisons of the monolayer coverage and stability across the tripod series and for the monovalent pyrene anchor are consistent with the hypothesis that the tripods adopt an upright conformation on the SLG surface. We also study the effect of shortening the four-carbon linker between the feet and tetrahedral core to a single methylene group. This change might be expected to weaken the tripod–SLG interaction by restricting the ability of all three feet to interact with the surface. However, we observe almost no change in density or monolayer stability between the two compounds, suggesting that the linker length may be selected based on synthetic convenience. This work represents a significant step forward in our understanding of molecular assembly on the graphene basal plane and of the design criteria required for the development of general binding motifs for the noncovalent functionalization of SLG.

RESULTS AND DISCUSSION

We previously evaluated the coverage and kinetic stability of the $Co(tpy)_2$-functionalized pyrene tripod **1a·2PF$_6$** and corresponding monopodal pyrene complex **2·3PF$_6$**. The phenanthrene and naphthalene tripods **1b·2PF$_6$** and **1c·2PF$_6$**, respectively, derive from a common alkyne precursor **3** (Scheme 1). Sonogashira cross-coupling between **3** and terpyridine **4**, followed by demethylation using BBr_3, provides tris(phenol) **5**. Williamson etherification of **5** with the appropriate polycyclic aromatic hydrocarbon (PAH) electrophile, followed by formation of the heteroleptic $Co(tpy)_2$ complex, provides the tripods **1a–c·2PF$_6$**. The Co^{2+} complexes are paramagnetic, complicating their characterization using NMR spectroscopy, but oxidizing them to the corresponding Co^{3+} oxidation state using $AgPF_6$ provides readily characterized diamagnetic species (see Supporting Information for experimental procedures and molecular characterization data). We also prepared two ferrocene-containing pyrene tripods, **7a** and **7b**, with a variable number of methylene spacers (4 or 1) between their pyrene feet and the tetrahedral core. Ferrocene was selected as an alternate redox couple because of its rapid electron transfer kinetics, ease of synthesis, and chemical stability. It was incorporated into tripods *via* intermediate **6**, which serves as a universal tripod precursor, to which arbitrary feet and functional head groups may be attached through orthogonal chemical reactions.

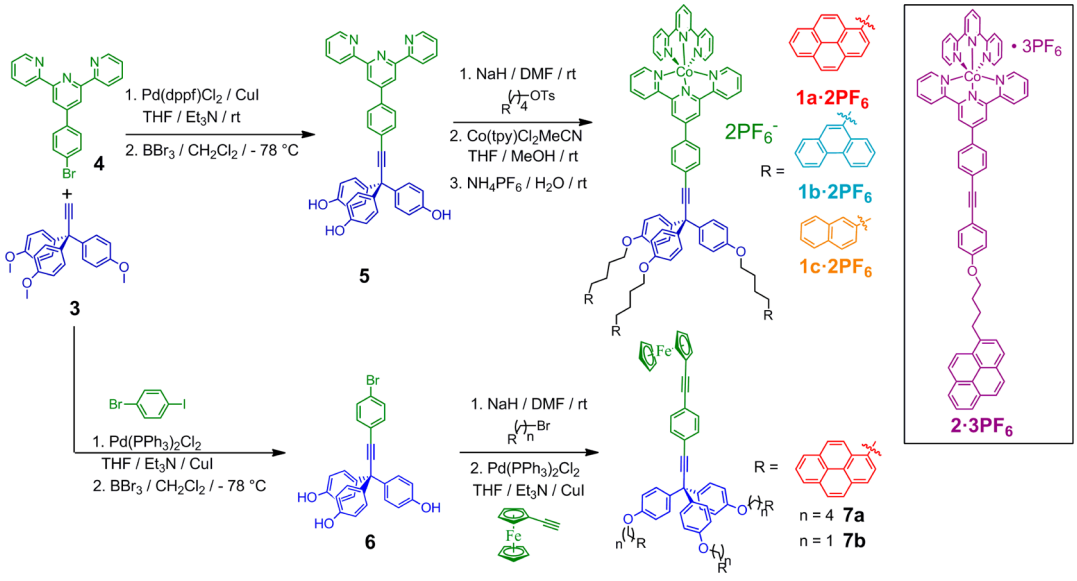

Scheme 1. The synthesis of 1a–c·2PF$_6$ and 7a–b

Cyclic voltammetry (CV) at SLG working electrodes [0.07 cm^2 active area, see Supporting Information for fabrication details; THF/*n*-Bu_4NClO_4 (0.1M) supporting electrolyte] of each of the above compounds (**1a**–**c**·**2PF$_6$**, Supporting Information Figures S35 and S36; **7a**–**b**, Figures S37 and S38) showed behavior consistent with electrode-bound redox couples. Compounds **1a**–**c**·**2PF$_6$** showed quasireversible electron transfer kinetics with peak separations of their oxidative and reductive waves (ΔE_p) *ca.* 100 mV at potential sweep rates of 0.1 V s^{-1}. Ferrocene compounds **7a**–**b** showed electrochemical reversibility, over the full range of scan rates examined (up to 0.5 V s^{-1}), as indicated by their ΔE_p of 0–60 mV (we attribute the variation of ΔE_p to variations in graphene electrode conductivity).[52,53] All five complexes exhibited complete chemical reversibility with consistent peak shape and height over many voltammetric cycles. The charge passed during oxidation and reduction is directly proportional to the monolayer density through the equation $\Gamma = Q(nFA)^{-1}$, in which Γ is the coverage, *n* is the number of electrons transferred, *Q* is the charge passed, *F* is the Faraday constant, and *A* is the electroactive area of the working electrode. We used CV to construct adsorption isotherms by determining the surface-bound molecular coverage as a function of the solution concentration of compounds **1a**–**c**·**2PF$_6$**. The isotherms were fit to the Langmuir model using the equation $\Gamma = \Gamma_s K_c(K_c + 1)^{-1}$, allowing extraction of the monolayer saturation coverage (Γ_s) and energy of adsorption (ΔG_{ads}, Figure 1A). Each of the binding groups exhibits a favorable ΔG_{ads} of *ca.* −39 kJ mol^{-1} (see Supporting Information Table S1), which is relatively strong for noncovalently bound species. However, the tripods show substantial variation in their saturation coverages. The pyrene tripod **1a**·**2PF$_6$** reaches saturation at Γ_s = 74 pmol cm^{-2}, corresponding to a footprint of 2.3 nm^2. The phenanthrene tripod **1b**·**2PF$_6$**, whose anchors contain one fewer aromatic ring, achieves substantially higher saturation coverage of Γ_s = 106 ± 6 pmol cm^{-2}, corresponding to a molecular footprint of 1.6 nm^2. The naphthalene anchored tripod **1c**·**2PF$_6$** follows the same trend with Γ_s = 114 ± 3 pmol cm^{-2}, corresponding to a molecular footprint of 1.5 nm^2. The pyrene monopod **2**·**3PF$_6$** reaches lower coverage than either **1b**·**2PF$_6$** or **1c**·**2PF$_6$** (Γ_s = 90.7 ± 0.6 pmol cm^{-2}), corresponding to a molecular footprint of 1.7 nm^2. The saturation coverages of the three tripod complexes scale linearly with the combined Connolly surface areas of their three feet, while the monolayers of **2**·**3PF$_6$** show lower than expected coverage based on the size of a single pyrene moiety (≈ 0.7 nm^2). This observation is consistent with our hypothesis that tripods adopt upright configurations, whereas molecules bearing a single pyrene are likely to lie flat to maximize their van der Waals contact to the surface. This conclusion is further

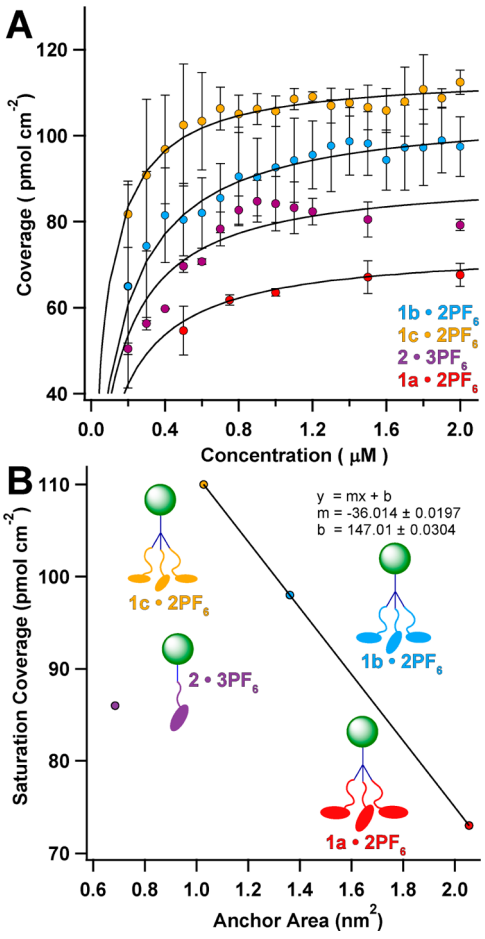

Figure 1. (A) Binding isotherms calculated from CV measurements of the coverage of 1a–c·2PF$_6$ at varying solution concentrations. Each data point represents the average of three measurements, and the error bars indicate one standard deviation from the average. (B) Plot of saturation coverage as a function of the combined Connolly surface areas of each binding group. This plot indicates that tripods form dense monolayers corresponding to their binding group size, while monofunctional pyrene binding group 2·3PF$_6$ shows reduced saturation coverage for its size.

supported by our previous comparison of electron transfer rate constants between SLG and **1a**·**2PF$_6$** and **2**·**3PF$_6$**.[48] Although the pyrene monopod achieves moderately higher coverage than the pyrene tripod, its coverage is lower than the tripods' anchored by smaller PAHs, which show saturation coverages consistent with dense monolayers (Figure 1B). These findings demonstrate that the multivalent tripod design is more effective than monovalent binding groups for organizing dense functionality on the SLG surface.

The stability of the monolayers of each complex shows a strong dependence on the size of its binding group. Differences in desorption rates were assessed by functionalizing SLG working electrodes with a monolayer of each complex, which was removed from the adsorbate solution and rinsed with fresh solvent to remove excess weakly bound molecules. After refilling the electrochemical cell with blank electrolyte solution, molecular desorption was quantified by performing

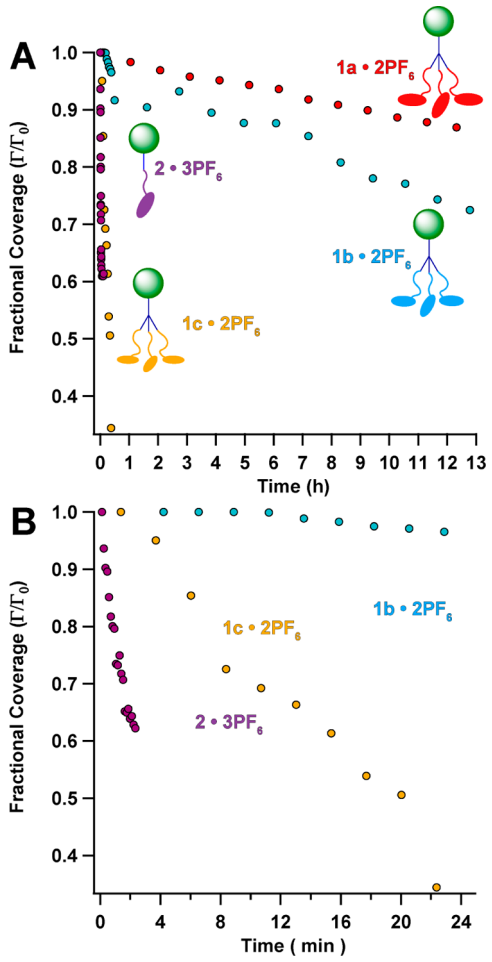

Figure 2. (A) Fractional coverage (Γ/Γ_0) of monolayers of 1a−c·2PF$_6$ and 2·3PF$_6$ over the course of 12 h after transfer to a blank electrolyte solution (THF/0.1 M NH_4ClO_4); (B) an expansion of the first 25 min of these desorption experiments indicates the differences in stability between 1b·2PF$_6$, 1c·2PF$_6$, and 2·3PF$_6$ (1a·2PF$_6$ not shown).

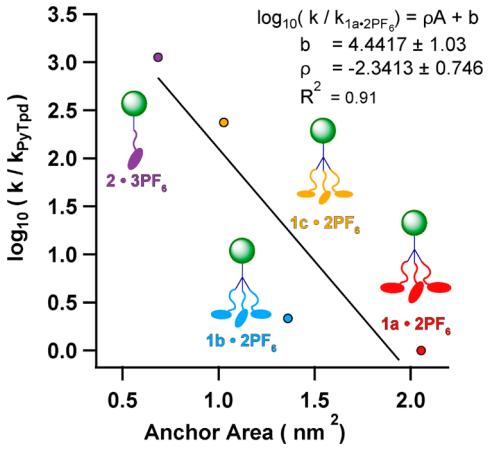

Figure 3. The rates of desorption of 1a−c·2PF$_6$ and 2·3PF$_6$ and the surface area available for binding to SLG exhibit a logarithmic relationship consistent with each tripod adopting multivalent van der Waals contact with the SLG basal plane.

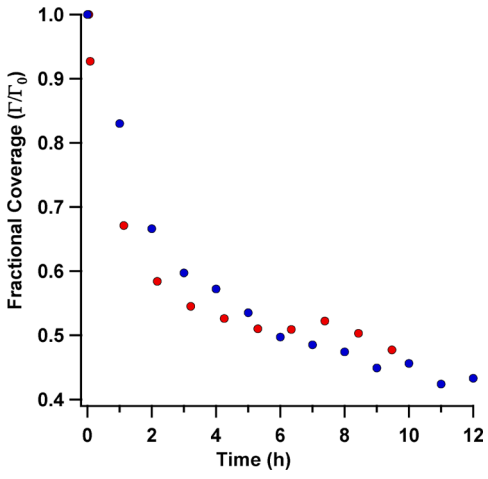

Figure 4. Fractional coverage (Γ/Γ_0) of monolayers of 7a (blue) and 7b (red) over the course of 12 h after transfer to a blank electrolyte solution (THF/0.1 M NH_4ClO_4). These data indicate similar desorption rates for ferrocone-containing pyrene tripods with either 1 or 4 methylene groups between their tetrahedral core and pyrene feet.

periodic CVs for up to 12 h (Figure 2). Panels A and B of Figure 2 show the resulting desorption curves for **1a**−**c·2PF$_6$** and the monopodal model compound **2·3PF$_6$** over the full time range and the first 25 min, respectively. The pyrene tripod **1a·2PF$_6$** is exceptionally stable, as it retains 86% of its initial coverage after 12 h, corresponding with desorption rate constant $k = 3.5 \times 10^{-6}$ s^{-1}. The phenanthrene tripod **1b·2PF$_6$** desorbs approximately twice as fast ($k = 7.0 \times 10^{-6}$ s^{-1}), the naphthalene tripod **1c·2PF$_6$** desorbs approximately 200 times more rapidly ($k = 6.2 \times 10^{-4}$ s^{-1}), and the monovalent compound **2·3PF$_6$** desorbs 1000 times faster ($k = 1.4 \times 10^{-3}$ s^{-1}). The differences in desorption rates exhibit a logarithmic relationship with the combined Connolly surface areas of each binding group (Figure 3), suggesting that the stability of future PAH-based binding motifs may be predicted from their van der Waals surface areas. In this way, the tripod design offers a means to achieve high surface-area contacts needed for stable monolayers without resorting to the use of giant PAHs, which generally show poor solubility and limited synthetic accessibility. Finally, it should be noted that these desorption rates correspond to infinite dilution conditions in good solvents for the binding groups. We anticipate that desorption will be slower in poor solvents for the tripod, including aqueous solutions, perhaps mitigating the trade-off between monolayer density and stability for tripods with smaller feet.

We also evaluated the effect on the monolayer coverage and stability to desorption of shortening the methylene chains linking the feet to the tetrahedral core. Ferrocene pyrene tripods **7a** and **7b** both showed saturation coverages of *ca.* 66 pmol cm^{-2}, almost identical to the Co(tpy)$_2$ analog **1a·2PF$_6$**. These coverages indicate that the anchor size, not the identity of the pendant redox couple, largely determines the molecular footprint and that the single methylene

spacer does not affect monolayer density significantly. **7a** and **7b** desorb from SLG with rate constants of 1.1×10^{-4} and 2.5×10^{-4} s^{-1}, respectively. These similar values reflect a tolerance of the shorter linker, and we conclude that the choice of linker length between 1 and 4 methylenes (and perhaps longer) may be guided by synthetic convenience rather than binding properties (Figure 4). It should be noted that **7a** and **7b** both desorb more rapidly than **1a**·$2PF_6$, which we attribute to the higher solubility (and therefore, more favorable solvent−solute interactions) of the ferrocene complexes. These results indicate that monolayer stability is not completely independent of the headgroup, such that larger feet might be needed to enhance monolayer stability as demanded by the specific headgroup and solvent required by specific future application constraints.

CONCLUSIONS

We have shown that tripodal motifs bearing various aromatic anchors spontaneously form kinetically and chemically stable monolayers on SLG from micromolar concentration solutions of organic solvents. The tripodal motif anchors functionality on graphene more efficiently than monofunctional anchors by forming densely packed monolayers that resist desorption effectively. By preparing and analyzing a series of tripods with different anchor sizes, we demonstrated a logarithmic relationship between anchor area and desorption rate, as well as a linear dependence of packing density on anchor size. In this way, the tripodal design provides a means to access high surface-area contacts needed for stable monolayers. Furthermore, modulation of the core-anchor linker length and the redox-active headgroup indicated that the binding characteristics are governed primarily, but not exclusively, by the total surface area of the PAH anchors. Together, these results provide a framework for designing and benchmarking new graphene binding motifs. Ongoing work will focus on utilizing tripodal compounds in SLG-based devices and exploring further modification of the tripod structures to enhance their binding characteristics while minimizing the molecular footprint size. These binding groups will provide the foundation for developing SLG as a useful analytical and sensing platform.

METHODS

Material Characterization. Infrared spectra of solid samples were recorded using a Thermo Nicolet iS10 FT-IR spectrometer with a diamond ATR attachment. Mass spectra were obtained on a Waters MALDI micro MX MALDI-TOF mass spectrometer using positive ionization in reflectron mode. NMR spectra were recorded on a Varian INOVA 400 MHz spectrometer using a ^{1}H/X Z-PFG probe, a Bruker ARX 300 MHz spectrometer using a BBO probe, a Varian INOVA 500 MHz spectrometer using a standard ^{1}H(^{13}C, ^{15}N) Z-PFG probe, or a Varian INOVA 600 MHz spectrometer using a standard ^{1}H(^{13}C, ^{15}N) XYZ-PFG probe with a 20 Hz sample spin rate.

Electrochemical Characterization. Electrochemistry experiments were performed on a Princeton Applied Research VersaSTAT 3 potentiostat using a standard three electrode configuration with graphene as the working-sense electrode, a Pt wire as the counter, and a Pt wire pseudoreference. The analyses were performed in a custom-made Teflon cell (Figure S1) that allowed exposure of a controlled area of the graphene electrode (Figure S2) (total area *ca.* 2 cm^2, exposed area *ca.* 0.07 cm^2). The supporting electrolyte was NBu_4ClO_4 in THF (0.1 M), and analysis was performed under ambient conditions (*i.e.*, oxygen and trace water).

Graphene electrodes were prepared by transferring single-layer graphene grown on Cu foil by chemical vapor deposition onto Si/SiO_2 wafers.[16] Electrical contact was made to the graphene by pressing a contact wire into a bead of In metal placed on the graphene surface outside of the electroactive region. All measurements used 1 mL of analyte solution. Cyclic voltammograms were recorded in analyte solution in every case, except desorption experiments, which used supporting electrolyte only.

Conflict of Interest: The authors declare no competing financial interest.

Supporting Information Available: Detailed synthetic procedures, spectroscopic characterization of new compounds, representative Raman spectra of the graphene electrodes used, and additional electrochemical characterization. This material is available free of charge *via* the Internet at http://pubs.acs.org.

Acknowledgment. We acknowledge financial support from Cornell University, a Sloan Research Fellowship, the Research Corporation for Science Advancement, and the Camille and Henry Dreyfus Foundation. We also acknowledge NSF support through use of the Cornell Nanofabrication Facility/NNIN and the Cornell Center for Materials Research facilities. J.A.M. gratefully acknowledges the Integrative Graduate Education and Research Traineeship (IGERT) Program in the Nanoscale Control of Surfaces and Interfaces which is supported under NSF Award DGE-0654193, the Cornell Center for Materials Research, and Cornell University.

REFERENCES AND NOTES

1. Novoselov, K. S.; Geim, A. K.; Morozov, S. V.; Jiang, D.; Zhang, Y.; Dubonos, S. V.; Grigorieva, I. V.; Firsov, A. A. Electric Field Effect in Atomically Thin Carbon Films. *Science* **2004**, *306*, 666–669.
2. Chen, J.-H.; Jang, C.; Xiao, S.; Ishigami, M.; Fuhrer, M. S. Intrinsic and Extrinsic Performance Limits of Graphene Devices on SiO_2. *Nat. Nanotechnol.* **2008**, *3*, 206–209.
3. Lee, C.; Wei, X.; Kysar, J. W.; Hone, J. Measurement of the Elastic Properties and Intrinsic Strength of Monolayer Graphene. *Science* **2008**, *321*, 385–388.
4. Liu, W.; Jackson, B. L.; Zhu, J.; Miao, C.-Q.; Chung, C.-H.; Park, Y. J.; Sun, K.; Woo, J.; Xie, Y.-H. Large Scale Pattern Graphene Electrode for High Performance in Transparent Organic Single Crystal Field-Effect Transistors. *ACS Nano* **2010**, *4*, 3927–3932.
5. Jang, S.; Jang, H.; Lee, Y.; Suh, D.; Baik, S.; Hong, B. H.; Ahn, J.-H. Flexible, Transparent Single-Walled Carbon Nanotube Transistors with Graphene Electrodes. *Nanotechnology* **2010**, *21*, 425201/1–425201/5.
6. Nair, R. R.; Blake, P.; Grigorenko, A. N.; Novoselov, K. S.; Booth, T. J.; Stauber, T.; Peres, N. M. R.; Geim, A. K. Fine Structure Constant Defines Visual Transparency of Graphene. *Science* **2008**, *320*, 1308–1308.
7. Yuk, J. M.; Park, J.; Ercius, P.; Kim, K.; Hellebusch, D. J.; Crommie, M. F.; Lee, J. Y.; Zettl, A.; Alivisatos, A. P. High-Resolution EM of Colloidal Nanocrystal Growth Using Graphene Liquid Cells. *Science* **2012**, *336*, 61–64.

8. Mohanty, N.; Fahrenholtz, M.; Nagaraja, A.; Boyle, D.; Berry, V. Impermeable Graphenic Encasement of Bacteria. *Nano Lett.* **2011**, *11*, 1270–1275.
9. Nair, R. R.; Blake, P.; Blake, J. R.; Zan, R.; Anissimova, S.; Bangert, U.; Golovanov, A. P.; Morozov, S. V.; Geim, A. K.; Novoselov, K. S.; *et al.* Graphene as a Transparent Conductive Support for Studying Biological Molecules by Transmission Electron Microscopy. *Appl. Phys. Lett.* **2010**, *97*, 153102.
10. Yan, Z.; Lin, J.; Peng, Z.; Sun, Z.; Zhu, Y.; Li, L.; Xiang, C.; Samuel, E. L.; Kittrell, C.; Tour, J. M. Toward the Synthesis of Wafer-Scale Single-Crystal Graphene on Copper Foils. *ACS Nano* **2012**, *6*, 9110–9117.
11. Bae, S.; Kim, H.; Lee, Y.; Xu, X.; Park, J.-S.; Zheng, Y.; Balakrishnan, J.; Lei, T.; Ri Kim, H.; Song, Y. I.; *et al.* Roll-to-Roll Production of 30-Inch Graphene Films for Transparent Electrodes. *Nat. Nanotechnol.* **2010**, *5*, 574–578.
12. Chen, S.; Cai, W.; Piner, R. D.; Suk, J. W.; Wu, Y.; Ren, Y.; Kang, J.; Ruoff, R. S. Synthesis and Characterization of Large-Area Graphene and Graphite Films on Commercial Cu–Ni Alloy Foils. *Nano Lett.* **2011**, *11*, 3519–3525.
13. Mattevi, C.; Kim, H.; Chhowalla, M. A Review of Chemical Vapour Deposition of Graphene on Copper. *J. Mater. Chem.* **2011**, *21*, 3324–3334.
14. Lee, Y.; Bae, S.; Jang, H.; Jang, S.; Zhu, S.-E.; Sim, S. H.; Song, Y. I.; Hong, B. H.; Ahn, J.-H. Wafer-Scale Synthesis and Transfer of Graphene Films. *Nano Lett.* **2010**, *10*, 490–493.
15. Li, X.; Cai, W.; An, J.; Kim, S.; Nah, J.; Yang, D.; Piner, R.; Velamakanni, A.; Jung, I.; Tutuc, E.; *et al.* Large-Area Synthesis of High-Quality and Uniform Graphene Films on Copper Foils. *Science* **2009**, *324*, 1312–1314.
16. Levendorf, M. P.; Ruiz-Vargas, C. S.; Garg, S.; Park, J. Transfer-Free Batch Fabrication of Single Layer Graphene Transistors. *Nano Lett.* **2009**, *9*, 4479–4483.
17. Reina, A.; Jia, X.; Ho, J.; Nezich, D.; Son, H.; Bulovic, V.; Dresselhaus, M. S.; Kong, J. Large Area, Few-Layer Graphene Films on Arbitrary Substrates by Chemical Vapor Deposition. *Nano Lett.* **2008**, *9*, 30–35.
18. Laaksonen, P.; Kainlauri, M.; Laaksonen, T.; Shchepetov, A.; Jiang, H.; Ahopelto, J.; Linder, M. B. Interfacial Engineering by Proteins: Exfoliation and Functionalization of Graphene by Hydrophobins. *Angew. Chem., Int. Ed.* **2010**, *49*, 4946–4949.
19. Kim, S. N.; Kuang, Z.; Slocik, J. M.; Jones, S. E.; Cui, Y.; Farmer, B. L.; McAlpine, M. C.; Naik, R. R. Preferential Binding of Peptides to Graphene Edges and Planes. *J. Am. Chem. Soc.* **2011**, 14480–14483.
20. Mannoor, M. S.; Tao, H.; Clayton, J. D.; Sengupta, A.; Kaplan, D. L.; Naik, R. R.; Verma, N.; Omenetto, F. G.; McAlpine, M. C. Graphene-Based Wireless Bacteria Detection on Tooth Enamel. *Nat. Commun.* **2012**, *3*, 763.
21. Wang, X.; Tabakman, S. M.; Dai, H. Atomic Layer Deposition of Metal Oxides on Pristine and Functionalized Graphene. *J. Am. Chem. Soc.* **2008**, *130*, 8152–8153.
22. Wang, Q. H.; Hersam, M. C. Room-Temperature Molecular-Resolution Characterization of Self-Assembled Organic Monolayers on Epitaxial Graphene. *Nat. Chem.* **2009**, *1*, 206–211.
23. Coletti, C.; Riedl, C.; Lee, D. S.; Krauss, B.; Patthey, L.; von Klitzing, K.; Smet, J. H.; Starke, U. Charge Neutrality and Band-Gap Tuning of Epitaxial Graphene on SiC by Molecular Doping. *Phys. Rev. B* **2010**, *81*, 235401–235409.
24. Alaboson, J. M. P.; Wang, Q. H.; Emery, J. D.; Lipson, A. L.; Bedzyk, M. J.; Elam, J. W.; Pellin, M. J.; Hersam, M. C. Seeding Atomic Layer Deposition of High-K Dielectrics on Epitaxial Graphene with Organic Self-Assembled Monolayers. *ACS Nano* **2011**, *5*, 5223–5232.
25. Cheng, H.-C.; Shiue, R.-J.; Tsai, C.-C.; Wang, W.-H.; Chen, Y.-T. High-quality Graphene P-N Junctions *via* Resist-Free Fabrication and Solution-Based Noncovalent Functionalization. *ACS Nano* **2011**, *5*, 2051–2059.
26. Lee, W. H.; Park, J.; Sim, S. H.; Lim, S.; Kim, K. S.; Hong, B. H.; Cho, K. Surface-Directed Molecular Assembly of Pentacene on Monolayer Graphene for High-Performance Organic Transistors. *J. Am. Chem. Soc.* **2011**, *133*, 4447–4454.
27. Jandhyala, S.; Mordi, G.; Lee, B.; Lee, G.; Floresca, C.; Cha, P. R.; Ahn, J.; Wallace, R. M.; Chabal, Y. J.; Kim, M. J.; *et al.* Atomic Layer Deposition of Dielectrics on Graphene Using Reversibly Physisorbed Ozone. *ACS Nano* **2012**, *6*, 2722–2730.
28. Lee, W. H.; Suk, J. W.; Lee, J.; Hao, Y. F.; Park, J.; Yang, J. W.; Ha, H. W.; Murali, S.; Chou, H.; Akinwande, D.; *et al.* Simultaneous Transfer and Doping of CVD-Grown Graphene by Fluoropolymer for Transparent Conductive Films on Plastic. *ACS Nano* **2012**, *6*, 1284–1290.
29. Colson, J. W.; Woll, A. R.; Mukherjee, A.; Levendorf, M. P.; Spitler, E. L.; Shields, V. B.; Spencer, M. G.; Park, J.; Dichtel, W. R. Oriented 2D Covalent Organic Framework Thin Films on Single-Layer Graphene. *Science* **2011**, *332*, 228–231.
30. Malig, J.; Jux, N.; Kiessling, D.; Cid, J.-J.; Vázquez, P.; Torres, T.; Guldi, D. M. Towards Tunable Graphene/Phthalocyanine–PPV Hybrid Systems. *Angew. Chem., Int. Ed.* **2011**, *50*, 3561–3565.
31. Sabri, S. S.; Guillemette, J.; Guermoune, A.; Siaj, M.; Szkopek, T. Enhancing Gas Induced Charge Doping in Graphene Field Effect Transistors by Non-Covalent Functionalization with Polyethyleneimine. *Appl. Phys. Lett.* **2012**, *100*, 113106/1–113106/4.
32. Yan, C.; Kim, K. S.; Lee, S. K.; Bae, S. H.; Hong, B. H.; Kim, J. H.; Lee, H. J.; Ahn, J. H. Mechanical and Environmental Stability of Polymer Thin-Film-Coated Graphene. *ACS Nano* **2012**, *6*, 2096–2103.
33. Love, J. C.; Estroff, L. A.; Kriebel, J. K.; Nuzzo, R. G.; Whitesides, G. M. Self-Assembled Monolayers of Thiolates on Metals as a Form of Nanotechnology. *Chem. Rev.* **2005**, *105*, 1103–1170.
34. Hofer, R.; Textor, M.; Spencer, N. D. Alkyl Phosphate Monolayers, Self-Assembled from Aqueous Solution onto Metal Oxide Surfaces. *Langmuir* **2001**, *17*, 4014–4020.
35. Gao, W.; Dickinson, L.; Grozinger, C.; Morin, F. G.; Reven, L. Self-Assembled Monolayers of Alkylphosphonic Acids on Metal Oxides. *Langmuir* **1996**, *12*, 6429–6435.
36. Badia, A.; Lennox, R. B.; Reven, L. A Dynamic View of Self-Assembled Monolayers. *Acc. Chem. Res.* **2000**, *33*, 475–481.
37. Ulman, A. Formation and Structure of Self-Assembled Monolayers. *Chem. Rev.* **1996**, *96*, 1533–1554.
38. Georgakilas, V.; Otyepka, M.; Bourlinos, A. B.; Chandra, V.; Kim, N.; Kemp, K. C.; Hobza, P.; Zboril, R.; Kim, K. S. Functionalization of Graphene: Covalent and Non-Covalent Approaches, Derivatives and Applications. *Chem. Rev.* **2012**, *112*, 6156–6214.
39. Hirsch, A.; Englert, J. M.; Hauke, F. Wet Chemical Functionalization of Graphene. *Acc. Chem. Res.* **2013**, *46*, 87–96.
40. Johns, J. E.; Hersam, M. C. Atomic Covalent Functionalization of Graphene. *Acc. Chem. Res.* **2013**, *46*, 77–86.
41. Park, J.; Yan, M. D. Covalent Functionalization of Graphene with Reactive Intermediates. *Acc. Chem. Res.* **2013**, *46*, 181–189.
42. Paulus, G. L. C.; Wang, Q. H.; Strano, M. S. Covalent Electron Transfer Chemistry of Graphene with Diazonium Salts. *Acc. Chem. Res.* **2013**, *46*, 160–170.
43. Lim, H.; Lee, J. S.; Shin, H.-J.; Shin, H. S.; Choi, H. C. Spatially Resolved Spontaneous Reactivity of Diazonium Salt on Edge and Basal Plane of Graphene without Surfactant and Its Doping Effect. *Langmuir* **2010**, *26*, 12278–12284.
44. Sun, Z.; Kohama, S.-i.; Zhang, Z.; Lomeda, J.; Tour, J. Soluble Graphene Through Edge-Selective Functionalization. *Nano Res.* **2010**, *3*, 117–125.
45. Yu, D. S.; Kuila, T.; Kim, N. H.; Khanra, P.; Lee, J. H. Effects of Covalent Surface Modifications on the Electrical and Electrochemical Properties of Graphene Using Sodium 4-Aminoazobenzene-4′-Sulfonate. *Carbon* **2013**, *54*, 310–322.
46. Guryel, S.; Hajgato, B.; Dauphin, Y.; Blairon, J. M.; Miltner, H. E.; De Proft, F.; Geerlings, P.; Van Lier, G. Effect of Structural Defects and Chemical Functionalisation on the Intrinsic Mechanical Properties of Graphene. *Phys. Chem. Chem. Phys.* **2013**, *15*, 659–665.
47. Bissett, M. A.; Tsuji, M.; Ago, H. Mechanical Strain of Chemically Functionalized Chemical Vapor Deposition Grown Graphene. *J. Phys. Chem. C* **2013**, *117*, 3152–3159.

48. Mann, J. A.; Rodríguez-López, J.; Abruña, H. D.; Dichtel, W. R. Multivalent Binding Motifs for the Noncovalent Functionalization of Graphene. *J. Am. Chem. Soc.* **2011**, *133*, 17614–17617.
49. Rodríguez-López, J.; Ritzert, N. L.; Mann, J. A.; Tan, C.; Dichtel, W. R.; Abruña, H. D. Quantification of the Surface Diffusion of Tripodal Binding Motifs on Graphene Using Scanning Electrochemical Microscopy. *J. Am. Chem. Soc.* **2012**, *134*, 6224–6236.
50. Mann, J. A.; Alava, T.; Craighead, H. G.; Dichtel, W. R. Preservation of Antibody Selectivity on Graphene by Conjugation to a Tripod Monolayer. *Angew. Chem., Int. Ed.* **2013**, *52*, 3177–3180.
51. Alava, T.; Mann, J. A.; Théodore, C.; Benitez, J. J.; Dichtel, W. R.; Parpia, J. M.; Craighead, H. G. Control of the Graphene−Protein Interface Is Required To Preserve Adsorbed Protein Function. *Anal. Chem.* **2013**, *85*, 2754–2759.
52. Keil, R. G. Resistive Electrode Effects on Cyclic Voltammetry. *J. Electrochem. Soc.* **1986**, *133*, 1375–1379.
53. García-Jareño, J. J.; Navarro-Laboulais, J.; Vicente, F. A Numerical Approach to the Voltammograms of the Reduction of Prussian Blue Films on ITO Electrodes. *Electrochim. Acta* **1997**, *42*, 1473–1480.